energies

MDPI

Article

Optimal Management of a Microgrid with Radiation and Wind-Speed Forecasting: A Case Study Applied to a Bioclimatic Building

Luis O. Polanco Vásquez [1], Víctor M. Ramírez [1,*], Diego Langarica Córdova [2], Juana López Redondo [3], José Domingo Álvarez [3] and José Luis Torres-Moreno [3]

[1] Unidad de Energía Renovable, Centro de Investigación Científica de Yucatán AC., Mérida 97205, Mexico; luis.polanco@estudiantes.cicy.mx
[2] Ingeniería Electrónica, Facultad de Ciencias, UASLP, San Luis Potosí 78295, Mexico; diego.langarica@uaslp.mx
[3] Agrifood Campus of International Excellence (ceiA3) CIESOL Joint Centre University of Almería-CIEMAT, 04120 Almería, Spain; jlredondo@ual.es (J.L.R.); jhervas@ual.es (J.D.Á.); jltmoreno@ual.es (J.L.T.-M.)
* Correspondence: victor.ramirez@cicy.mx; Tel.: +52-999-930-07-60

Abstract: An Energy Management System (EMS) that uses a Model Predictive Control (MPC) to manage the flow of the microgrids is described in this work. The EMS integrates both wind speed and solar radiation predictors by using a time series to perform the primary grid forecasts. At each sampling data measurement, the power of the photovoltaic system and wind turbine are predicted. Then, the MPC algorithm uses those predictions to obtain the optimal power flows of the microgrid elements and the main network. In this work, three time-series predictors are analyzed. As the results will show, the MPC strategy becomes a powerful energy management tool when it is integrated with the Double Exponential Smoothing (DES) predictor. This new scheme of integrating the DES method with an MPC presents a good management response in real-time and overcomes the results provided by the Optimal Power Flow method, which was previously proposed in the literature. For the case studies, the test microgrid located in the CIESOL bioclimatic building of the University of Almeria (Spain) is used.

Keywords: microgrid; EMS; MPC; control; simulation

Citation: Vásquez, L.O.P.; Ramírez, V.M.; Langarica Córdova, D.; Redondo, J.L.; Álvarez, J.D.; Torres-Moreno, J.L. Optimal Management of a Microgrid with Radiation and Wind-Speed Forecasting: A Case Study Applied to a Bioclimatic Building. *Energies* **2021**, *14*, 2398. https://doi.org/10.3390/en14092398

Academic Editor: Anastasios Dounis

Received: 18 March 2021
Accepted: 16 April 2021
Published: 23 April 2021

1. Introduction

The energy supplied for microgrids is produced mainly from renewable energy sources since they provide energy without significant carbon dioxide emissions. However, the challenge with these sources is the uncertainty they introduce to the electrical systems due to the variation of climatological conditions. It is essential to mitigate this problem and adapt it to the electrical systems. Commonly, the typical solution proposed is to buffer the output using energy storage systems (ESS) [1–3].

With the growth of microgrids and their implementation in electrical transport systems, the development of new control strategies is required to manage aspects related to both the intermittence and distribution of the generation as well as new consumption profiles [4]. Therefore, the algorithm that is implemented for control in energy management systems (EMS) must be developed with novel techniques to improve the efficiency of microgrids [5,6]. The microgrid requires an EMS to efficiently manage the power flows from the microgrid's different power sources. An EMS can cause many benefits, as increasing stability in voltage levels, reducing costs, reducing carbon emissions, and improving battery health [7]. EMSs are the key to efficiently manage the energy in Renewable Distributed Generation (RDGs) where microgrids are integrated. Therefore, the study of control strategies to improve their performance is of real interest. Several works have been carried out on the related control and optimization techniques.

The state-of-the-art nature of this work includes recent research on EMS that introduces different control and optimization techniques for energy management. Some research examples are described below. Hooshmand et al. [8,9] presented a stochastic MPC for energy management in a microgrid. In this work, the microgrid was integrated by a wind turbine as a renewable source, a fuel cell, a gas pipe, a storage system, and the load through the clients. The objective of this work was to manage energy reliably to supply it to customers. EMS tries to use renewable sources as much as possible, keeps the storage system fully charged, and reduces the gas turbine's energy. The resolution of the MPC is made through dynamic programming (DP). The advantage of using DP is that its complexity does not increase proportionally to the problem's size. Additionally, the DP method can be adapted to handle stochastic terms, named stochastic dynamic programming methods (SDP). Using an illustrative example, the work shows the validity of the implemented method.

K/bidi et al. [10] presented power management of a hybrid microgrid combining solar photovoltaic energy with an ESS under hydrogen cell technology to ensure long-term energy availability for microgrids. Hydrogen cells seem to be an interesting candidate; the paper proposes a control strategy dedicated to the integration of hydrogen storage in microgrids for better utilization of photovoltaic production. In [11,12], Morstyn et al. proposed an MPC for OPF between distributed battery energy storage systems in a DC microgrid. A new convex formulation of the DC microgrid OPF problem is used by modeling the static current, static voltage and power flows approximations. The corresponding optimization problem includes the losses and distribution lines and the voltage drops. Taking advantage of the existence of fast and robust solvers for convex optimization, a scalable solution for a real-time model can be obtained. To verify the correct operation of the strategy, real-time simulations were performed with a DC microgrid with a real-time digital simulator from RTDS Technologies.

Another strategy for EMS development is high-level MPC using Sliding Mode Control (SMC). It constructs a control function in an arbitrarily long-term horizon from an iterative solution of a finite horizon optimal control problem. The strategy is popular in control engineering, where it is known as sliding horizon MPC. This technique is also used to solve problems in mathematical economics under the name of the sliding plan. Moreover, in the investigation of operations such as the rolling horizon [13,14], Incremona et al. [15] proposed a MPC including a supervisory control structure with a Sliding Mode Control (SMC). The strategy was integrated into the EMS for the efficient management and consumption of energy. In the document, the microgrid included a photovoltaic system as a distributed unit and two energy storage units that operated autonomously and non-autonomously that was controlled by the MPC-SMC, which generates the power reference for energy storage systems, considering entry and status restrictions. The proposed approach was theoretically analyzed, and the asymptotic stability of the controlled system was ensured. The proposed effectiveness was confirmed throughout the evaluation of the simulations.

The estimation of uncertainties caused by climatic variables is vital for the control and optimization of energy in renewable sources. Making predictions on these variables with an acceptable degree of error is tolerable to compensate for future effects on the microgrid's decision variables. Uncertainties can force continuous variation of the control signal and generally require specific control strategies to minimize their influence. The main climatic variables that are used mostly in the generation of renewable energy are solar radiation and wind speed, since solar photovoltaic, thermal, and wind energy are among the most used in microgrids as renewable sources [16]. The use of solar and wind energy requires the forecast of solar radiation and wind speed in short time horizons (5, 10, 15, 30, and 60 min) to be able to feedback to the controls at adequate times to respond to the uncertainties that this type of energy source can present. Forecast models can be built using Autoregressive Integrated Moving Average (ARIMA), neural networks, a Kalman Filter, or Double Exponential Smoothing (DES). The models estimated the uncertainties

over the history before the start of the forecast horizon, the data was then forecasted, and finally, the predicted values were compared to the actual results [17].

Several methods to predict solar radiation and wind speed based on time series are considered in this work. More precisely, the Kalman filter, the Double Exponential Smoothing (DES) method and the Persistence Skill Score (PSS) method have been implemented. It should be noted that the last method was included in the study as a reference method, i.e., we will consider that a technique provides a good prediction if the corresponding error is less than that of PSS. As the results will show, the method with the best solutions for predicting solar radiation and wind speed is the DES method. It uses two dimming constants, the former is the average dimming constant of the data and the other is a dimming constant of the data trend, which is used for short-term forecasts that can be hours. This method is applied to a MPC and integrated into the EMS, which will manage the energy of a microgrid located in the CIESOL bioclimatic building of the University of Almería (Spain).

The management is carried out by minimizing a function of the economic cost of the energy. This work's main contribution is the integration of methods of prediction of climatic variables in a MPC controller that performs the function of an EMS in a microgrid by optimally managing energy flows. It allows for the improvement of the short-term control of EMS energy management. When using predictive control strategies, not only it is necessary to know the effects of these uncertainties, but future estimates of uncertainties would also be very useful to advance forecasting capabilities. The prediction methods used in the paper have two main objectives: to detect the stochastic nature of any variable represented as time-series data, and second, to forecast future behavior based on acquired data series. Furthermore, the prediction methods integrated into the MPC become a powerful tool for energy management in the EMS implemented for a microgrid.

The work is organized as follows. In Section 2, the mathematical models of the time series prediction methods used to forecast solar radiation and wind speed are explained. Additionally, an analysis to determine the best predictor is included. In Section 3, the MPC implemented for the EMS of the microgrid proposed in this work is described; for this reason, the mathematical formulation used for the MPC is carried out and the models used for this microgrid are also briefly explained. In Section 4, the methodology for the design of the simulations performed in this work is briefly described. Section 5 details the results obtained from the optimal operation of the considered microgrid. Finally, Section 5 summarizes the main conclusions inferred from the work.

2. Solar Radiation and Wind Speed Forecasting

In this work, solar radiation and wind speed predictors are developed with methods based on time series. In particular, the considered methods are the Double Exponential Smoothing (DES), Kalman filter, and Persistence Skill Score (PSS) methods. This section briefly describes them. To do so, we will denote z_{tk} as the measure at discrete time k and x_k as the predicted value one sample ahead.

2.1. Double Exponential Smoothing (DES)

The exponential smoothing function is a simple method for smoothing time series data; it assigns exponentially decreasing weights over time [18]. This method is appropriated for data that does not have a predictable upward and downward trend. DES continually reviews the estimated value in light of more recent experiences and is also based on smoothing the past values of a series in decreasing exponential form [19]. The DES is described by the following equations:

$$S_{tk} = \alpha y_{tk} + (1+\alpha)(S_{tk-1} + b_{tk-1}),\ 0 \leq \alpha \leq 1 \tag{1}$$

$$b_{tk} = \gamma(S_{tk} + S_{tk-1})(1+\gamma)b_{tk-1,}\ 0 \leq \gamma \leq 1 \tag{2}$$

$$F_{1+tk} = S_{tk} + b_{tk} \tag{3}$$

$$F_{m+tk} = S_{tk} + mb_{tk} \tag{4}$$

where S_{tk} represents the attenuated or ordered value at the origin, represented in Equation (1), α is an attenuation constant of the average of the data, and y_{tk} represents the actual measured data, b_{tk} is the trend value of period tk or slope of the line equation, represented in Equation (2), γ represents the trend estimation attenuation constant. In Equation (3), F_{1+tk} represents the prediction forecast of the variable of one period ahead, In Equation (4), F_{m+tk} represents the prediction forecast of the variable of m period ahead.

2.2. Kalman Filter

The Kalman filter algorithm solves the estimation problem in state variables in a dynamic system and can apply to physical, mathematical, economic, and climatological systems. It optimally solves the problem considering the noise generated by the measured variables, such as in the case of the weather, the pyrometers' measurements. This filter is applied when the systems are linear and have an equation of state [20]. The measurement equation describes how the measurements received from the sensors related to the equations of state must be described in discrete time. The dynamics of the measured variable's model must be formulated as the state equations shown in Equation (5) to apply the Kalman filter; Equation (6) shows us how the measurements we receive from the sensors are related to the equations of state of the system [21].

$$x_{tk} = Ax_{tk-1} + Bu_{tk-1} + w_{tk-1} \tag{5}$$

$$z_{tk} = Hx_{tk} + v_{tk} \tag{6}$$

In Equation (5), x_{tk} represents the state vector, A is the transition matrix, B represents the control matrix, u is the control vector, and w represents the noise of the system. Equation (6) represents the measurement equation where z_{tk} is the measurement vector, H is the random measurement matrix, and v_{tk} represents the measurement noise.

The Kalman filter algorithm estimates the state variables in real-time. As shown in Figure 1, it implements an infinite cycle that consists of receiving new information from the sensors and generating new data for the system. Each particular iteration has two stages: the prediction phase and the correction phase. The former step generates an a priori estimation representing a prediction of where our system should be working using the information from the dynamic model or equation of state by considering the estimation of previous instants, but without considering the data provided by the sensors [22]. The correction phase generates a posterior estimate that takes the a priori estimate and corrects it using the sensors' information. Neither step alone can produce a reasonable estimation. The variables with the subscripts denote a priori estimates, while those without it are posterior. Figure 1 clarifies how each of the matrix's A, B, and H are updated at each period of time to make the predictions and corrections to deliver a good estimate.

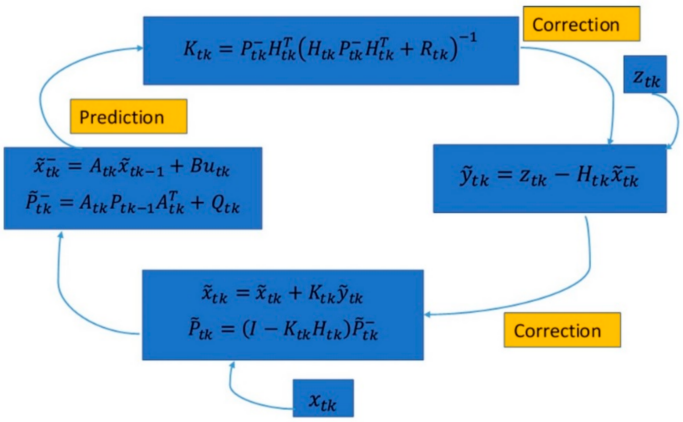

Figure 1. Kalman's filter algorithm.

2.3. Persistence Skill Score (PSS)

The Persistence Skill Score (PSS), commonly known as the persistent forecasting model, assumes that the values of solar irradiation and wind speed in the next period are the same as the previous one. Equation (7) describes the calculation of future value, where y is the measurement of the variable [23,24].

$$y^{tk} = y^{tk+1} \tag{7}$$

The PSS assumes that current mean data equals future predictions. The main weakness of this approach is the delay between the prediction time and the observation [24].

2.4. Validation Methods

In this subsection, the performance of the predictors is analyzed. To do so, the obtained results are statistically compared using the mean square error (MSE), the root mean square error (RMSE) and normalized RMSE (nRMSE). These three measurements have been computed to predict solar radiation and wind speed for a clear summer day and a cloudy winter day, both for the city of Almeria (Spain) [25].

A value of MSE close to zero indicates that the estimator x_{tk} predicts the observations of the parameter z_k with good precision; z_{tk} data are obtained through the measurements of the meteorological station in the bioclimatic building of CIESOL. Then, the model that obtains the smallest MSE is interpreted as the best, i.e., the one explaining the variability of the observations in the best way. RMSE measures the differences between the MSE values predicted by an estimator or predictor and the observed values [26]. Finally, the nRMSE metric is used for the sake of comparison. Equations (8)–(10) show how to calculate them.

$$\text{MSE} = \frac{1}{N}\sum_{k=1}^{N}(\hat{x}_{tx} - z_{tk})^2 \tag{8}$$

$$\text{RMSE} = \sqrt{\frac{1}{N}\sum_{k=1}^{N}(\hat{x}_{tk} - z_{tk})^2} \tag{9}$$

$$\text{nRMSE} = \frac{\sqrt{\frac{1}{N}\sum_{tk=1}^{N}(\hat{x}_{tk} - z_{tk})^2}}{\frac{1}{N}\sum_{tk=1}^{N}(z_{tk})^2} \tag{10}$$

Table 1 shows the obtained results by the three prediction techniques for solar irradiation (resp. wind speed) for a summer and a winter day. The forecast horizon was set to 10 samples for all the experiments. As can be seen, DES is the prediction technique for obtaining the lowest values for all the metrics, independently of the case of the study considered. The KF method is the second to show a better performance, with the MSE, RMSE, and nRMSE values inferior to PSS. As expected, the PSS obtains the poorest results. Nevertheless, it helps as a validation method to show the viability of the remaining methods. In this sense, we calculated the percentage of improvement.

For the sake of completeness, the obtained predictions are depicted in Figure 2. In particular, Figure 2a shows solar irradiation prediction results for a clear summer day. As can be visually observed, DES is the method with the best performance when predicting solar irradiation. Similar conclusions can be inferred for the winter day results (see Figure 2b). DES continues to be the best predictor for solar radiation. On the contrary, the Kalman filter is not as accurate, which might be due to this method's dependency on the model, and for the case at hand, the model does not describe the data behavior.

Table 1. Performance and comparison for statistics metrics.

			DES	Kalman Filter	PSS
Solar Irradiation	Summer day	MSE	3.4866	181.7	1318.5
		RMSE	1.8673	13.479	36.311
		nRMSE	0.0032877	0.023734	0.063933
	Winter day	MSE	160.68	4441.2	7408.8
		RMSE	12.676	66.642	86.074
		nRMSE	0.033513	0.17619	0.22756
Wind	Summer day	MSE	0.0036451	0.38061	0.48657
		RMSE	0.060375	0.61694	0.69755
		nRMSE	0.025121	0.25669	0.29023
	Winter day	MSE	0.055068	1.034	1.2691
		RMSE	0.23467	1.0168	1.1265
		nRMSE	0.061423	0.26615	0.29487

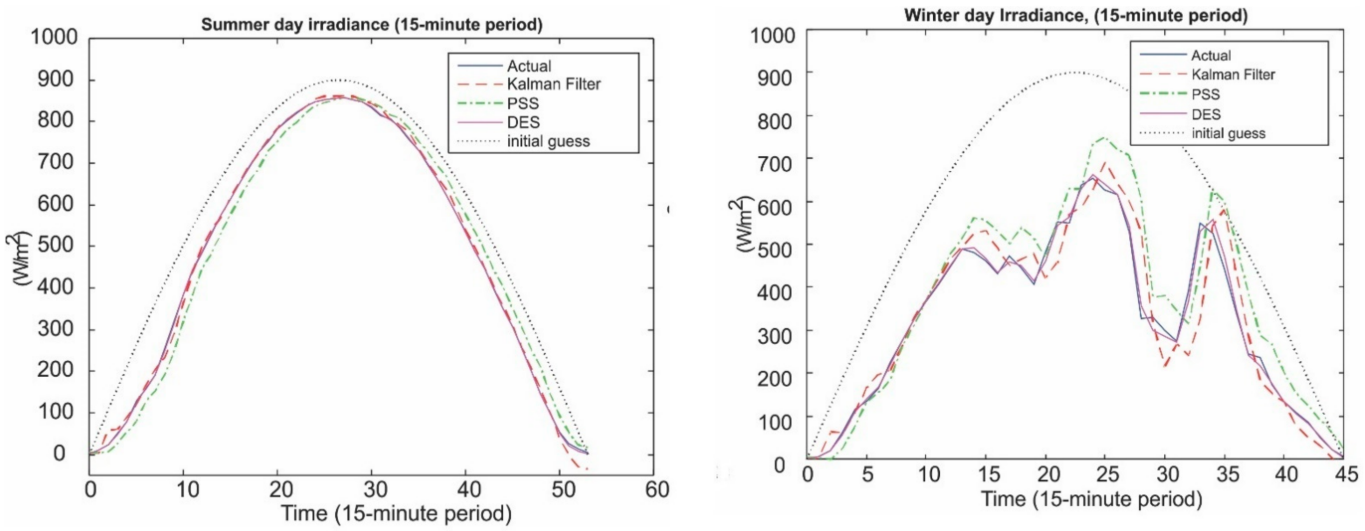

(**a**) (**b**)

Figure 2. Solar irradiation prediction. (**a**) Summer day irradiance, (**b**) Winter day irradiance.

Similarly, Figure 3 shows the predictions obtained by the three techniques for wind speed and the two different days considered (see Figure 3a,b, respectively). Again, we can visually observe that DES is superior to the other methods.

Therefore, according to the table results and visually confirmed by the figures, we can conclude that the best predictor for solar irradiation and wind speed is DES. Then, it will be used for the implementation of the MPC.

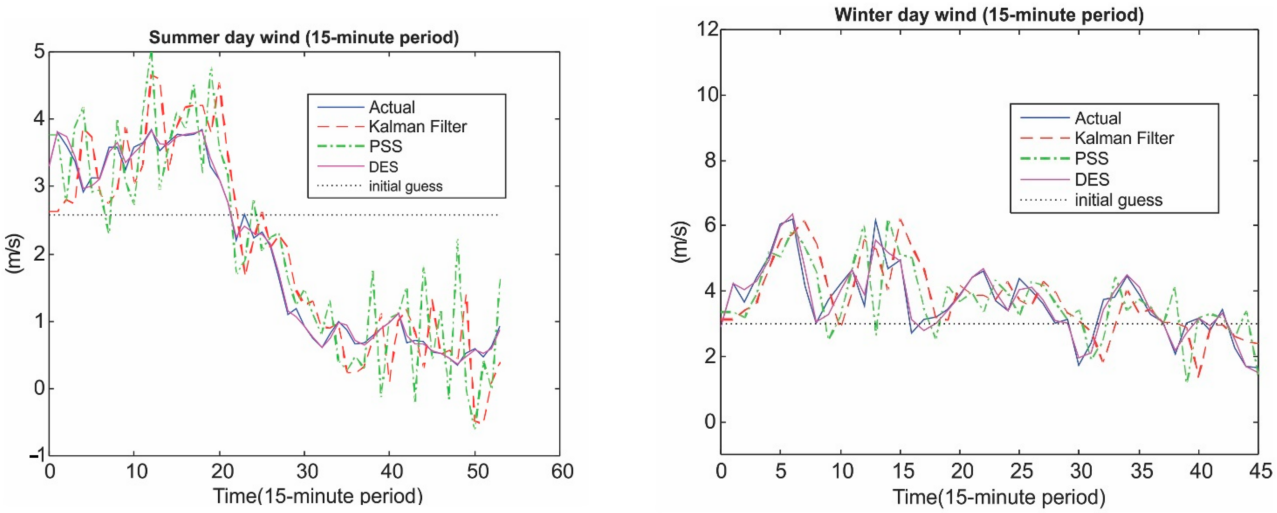

(**a**) (**b**)

Figure 3. Wind speed prediction. (**a**) Summer day wind, (**b**) Winter day wind.

3. Model-Based Predictive Control (MPC)

This section of the work describes the formulation of the control strategy: an MPC for the EMS in a microgrid, in which it is posed as an optimization problem solved by GA (Genetic Algorithm) [27–29]. One of the main challenges in the management of the microgrid energy is the external disturbances due to the use of renewable energy sources such as solar and wind power. The MPC is presented as a reliable, solid, and valid solution to counteract the uncertainties found in microgrids if a predictor for these disturbances is available and integrated into the MPC structure. This methodology has been used successfully in electrical power systems [30,31].

In Figure 4, the structure of the EMS is proposed for this work. As depicted, the commands generated by the EMS are sent to the converters, then the prediction information is sent to the MPC controller, which can predict the outputs of the disturbances concerning the microgrid. The converters used for this work are a buck–boost converter for the connection of the photovoltaic system, a bi-directional buck–boost converter for the charge and discharge of the storage system, and a buck–boost converter for the wind turbine. The interface block represents the flow of information between the microgrid sensors and the MPC.

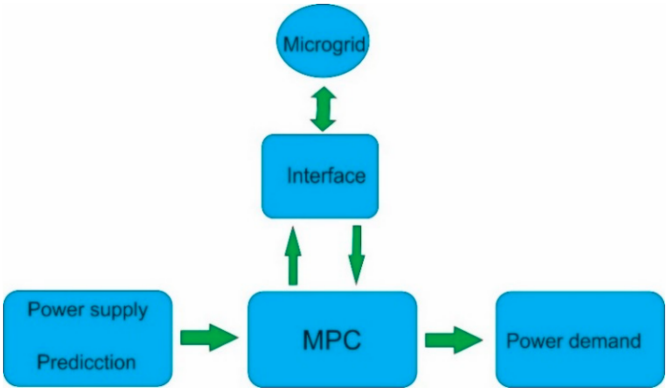

Figure 4. The structure of an EMS (Correct prediction, square on the left).

One of the main features of MPCs is the prediction of the output of the process that wants to be controlled, $\hat{y}(t+tk|t)$ during a prediction horizon N, for $k = 1$ to N, as a

function of the control sequence that is optimized, $u(t + tk - 1|t)$ [32]. The MPC includes a receding horizon strategy; that is, each time the horizon is displaced towards the future, once the optimal control sequence has been calculated, the first control signal for $k = 1$, $u(t)$, is applied and the remainder is discarded so the control sequence is recalculated at the next time instant, $k = 2$, with new and updated information [33] (Figure 5).

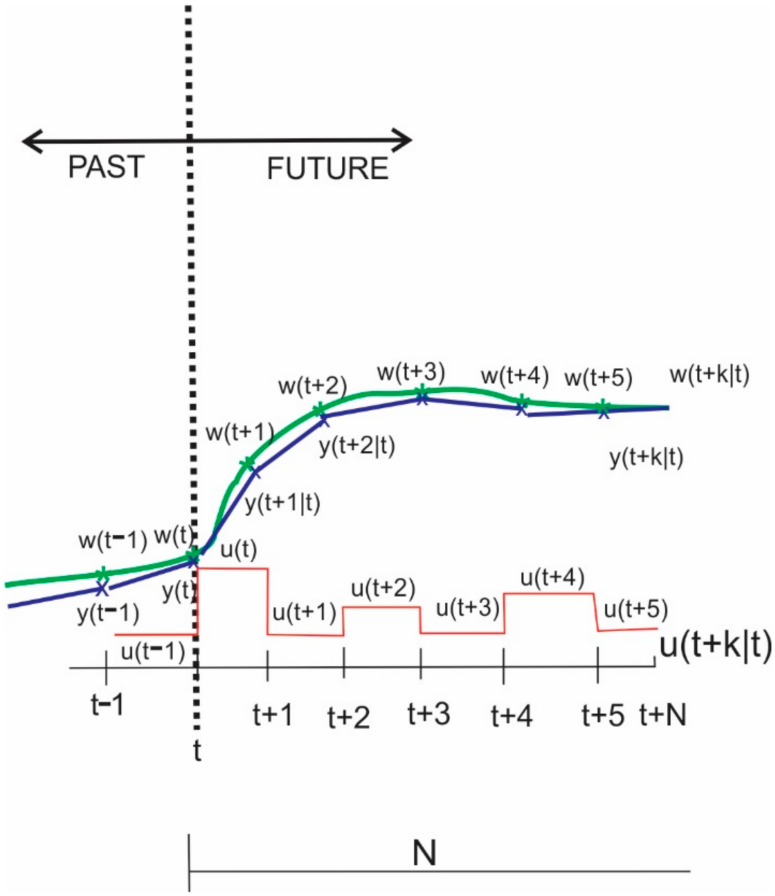

Figure 5. MPC.

Where in Figure 5 $w(t + tk|t)$ is the desired setpoint or reference that must be followed by the output of the controlled process and $y(t + tk|t)$ is the real output of the controlled process.

The mission of EMS is to minimize the cost of power per stage for a finite duration of time. The cost to be minimized in this work is the power taken from the main grid, which is described by Equation (11).

$$C_T = \sum_{t_k=1}^{N} \sum_{j=1}^{N_{ccp}} a_j + b_j\left(P_{MG_j}^{t_k}\right) + c_j\left(P_{MG_j}^{t_k}\right)^2 \tag{11}$$

where the cost of imported power from the network is denoted by C_T in €/h during a period T. Terms a, b, and c are cost-efficient assigned to conventional energy sources that are generally used by the main grid, and P_{MG} is the power imported from the main grid to the microgrid [34,35]. With these coefficients, we will identify the marginal propensity of maintenance expenses concerning the energy generation of each element of the microgrid. Also N_{ccp} denotes the common coupling point of the microgrid and the main grid.

Several equality constraints are added to the optimization problem to have the balance of active and reactive power [36], the current levels at the panel terminals as observed in Equation (12).

$$\boldsymbol{h}^{t_k}\left(\boldsymbol{x}^{t_k}\right) = \left\{ \begin{array}{c} P^{t_k}_{MGj} + \sum\limits_{\forall j} P^{t_k}_{Bcj} + \sum\limits_{\forall j} P^{t_k}_{Bdj} + \sum\limits_{\forall j} P^{t_k}_{wj} + \\ \sum\limits_{\forall j \in i} P^{t_k}_{CDj} - \sum\limits_{\forall j \in i} P^{t_k}_{lj} - \sum\limits_{\forall j \in i | j \in N_{Al}, N_T} P^{t_k}_{inj\ j}(\boldsymbol{V}, \boldsymbol{\theta}) = 0, \\ Q^{t_k}_{MGj} - \sum\limits_{\forall j} Q^{t_k}_{lj} - \sum\limits_{\forall j} Q^{t_k}_{inj\ j}(\boldsymbol{V}, \boldsymbol{\theta}) = 0 \\ j = 1, 2, \ldots, N_{bAC}; = 1, 2, \ldots, N_{bAC} | \forall j \notin N_{GEN} \\ \Delta I^{t_k}_{CDm} = I^{t_k}_{CDm} - f_{CD}\left(V^{t_k}_{CDm}, I^{t_k}_{CDm}\right) = 0 \\ \Delta P^{t_k}_{CDm} = P^{t_k}_{CAm}(\boldsymbol{V}, \boldsymbol{\theta}) - \Delta P^{t_k}_{CDm}\left(V^{t_k}_{CDm}, I^{t_k}_{CDm}\right) = 0 \\ \Delta V^{t_k}_{CDm} = V^{t_k}_{CDm} - \left(\frac{\pi}{16}\right) V^{t_k}_{m} = 0 \\ m = N_{bAC} + 1, \ldots, N_{bAC} + N_{bCD} \end{array} \right\} \forall t_k \in T \quad (12)$$

Inequality constraints are also added to handle the transitions between the charge and discharge of the battery or state of charge (SOC). These are observed in Equation (13); other restrictions are added to handle the voltage levels and the phase angle values to keep them within acceptable values for the operation, which are expressed in Equation (14) [37].

$$\boldsymbol{z}^{t_k}\left(\boldsymbol{x}^{t_k}\right) = \left\{ SOC^{min}_{Bj} \leq SOC^{t_k}_{Bj} \leq SOC^{max}_{Bj} \right\} \forall j \in N_B, \forall t_k \in T \quad (13)$$

$$\left\{ \begin{array}{c} \underline{\boldsymbol{y}}_{MG} \leq \boldsymbol{y}^{t_k}_{RD} \leq \overline{\boldsymbol{y}}_{MG} \\ \underline{\boldsymbol{y}}_{CD} \leq \boldsymbol{y}^{t_k}_{CD} \leq \overline{\boldsymbol{y}}_{CD} \\ \underline{\boldsymbol{y}}_{B} \leq \boldsymbol{y}^{t_k}_{B} \leq \overline{\boldsymbol{y}}_{B} \\ \underline{\boldsymbol{y}}_{W} \leq \boldsymbol{y}^{t_k}_{W} \leq \overline{\boldsymbol{y}}_{W} \end{array} \right\} \forall t_k \in T \quad (14)$$

To solve the optimization problem for MPC, the constraints introduced by mathematical models of batteries and renewable energy elements significantly affect the performance of the optimization algorithm [13]. This problem is very common for MPC, as this control strategy approximates the optimal infinite-horizon continuous-time domain control by repeatedly solving an optimal finite-horizon discrete-time open-loop control [38,39]. We can conclude that for this paper, an MPC with a longer horizon and a shorter sampling time is better since the optimization is completed in a sufficiently short time to be considered in real-time [40]. The mathematical models used in this work for the components of the microgrid are statics and can be consulted in the following paper for more details [41].

The energy cost data was obtained from OMIE (https://www.omie.es/es/ (accessed on 22 December 2020)), which is the electricity market operator designated for the management of the daily and intraday electricity market in the Iberian Peninsula. The aim of OMIE is to manage the daily and intraday wholesale electricity market (intraday and continuous intraday auctions) for Spain and Portugal [42].

4. Computational Simulation

4.1. Simulation Framework

In this work, the testbed microgrid located at the CIESOL bioclimatic building in the University of Almeria (Spain) was selected to validate the integration of the DES prediction method and the MPC. Such a microgrid is made up of a grid-tied solar photovoltaic (PV) system of 2 kW, a lead-acid storage system (battery) of 1 kW, a wind turbine of 1 kW, and a diesel generator of 2 kW. The scheme of the microgrid is shown in Figure 6. The parameters considered in the models of the components of this microgrid, as well as the cost coefficients associated with the energy imported through the main grid, are presented in Appendix A. The microgrid was simulated with MATLAB® R2015a software.

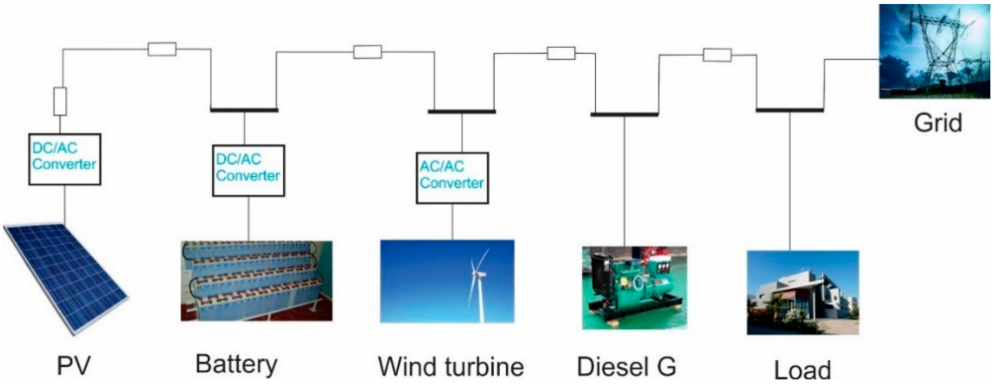

Figure 6. Scheme of the microgrid test used for the experiments.

Furthermore, according to the results presented in Section 2, the DES method was considered for predicting solar radiation and the wind speed.

Simulations were performed using an HP Pavilion Laptop with AMD Ryzen 33300U processor; the computer includes a Radeon Vega 2.10 GHz graphics card and 12 GB RAM.

A clear summer day in the city of Almería was considered as input for the simulation in this work. Figure 7a–c show the corresponding profiles of solar radiation, the wind speed, and the CIESOL building's standardized demand profile that can be consulted at [43], respectively. Additionally, in Figure 7a,b, the predictions obtained by DES method are also depicted in dashed red lines.

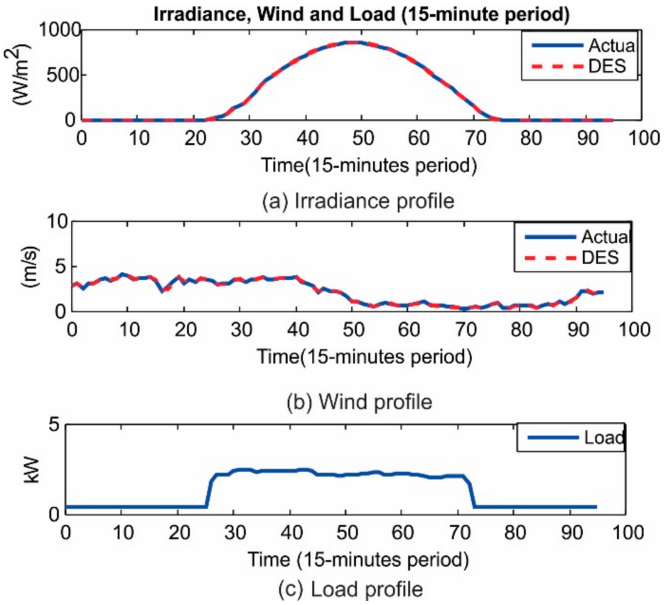

Figure 7. Forecasting curves for the testbed microgrid.

4.2. Results and Discussion

In the context previously described, a preliminary experiment was carried out to analyze the influence of the prediction horizon in the EMS results. To this aim, three simulations with three different prediction horizons have been accomplished. In particular, N = 5, 10, 15 (resp. 1 h 15′, 2 h 30′ and 3 h 45′) were set. The EMS performance was measured in terms of (i) efficiency, by saving the computational time, and (ii) effectiveness, by providing the final values of the power cost associated with the minimization of Equation (11), with an error tolerance of 1×10^{-9} for the constrains and 1×10^{-9} for the target function.

Figure 8 summarizes the obtained results. As can be seen, the greater the prediction horizon N is, the larger the computation time and the better the optimization results. Thus, a tradeoff between the solution's quality and the computational time is required to implement the MPC in real-time. For the work at hand, we considered such an equilibrium is achieved when N = 10 (2:30 h).

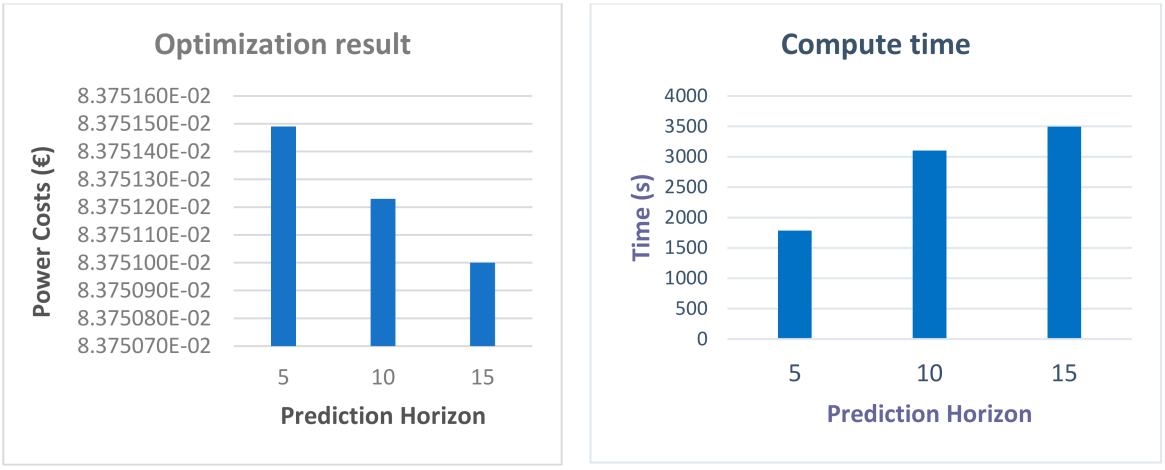

(**a**) (**b**)

Figure 8. Performance analysis of the EMS for different prediction horizons. (**a**) Optimization result, (**b**) Compute time.

Once the best prediction horizon was shown for the problem at hand, is N = 10 (2:30 h), the simulation of the EMS was carried out. The corresponding results are depicted in Figure 9. As can be seen, the battery takes advantage of charging when the wind turbine and photovoltaic system produce a surplus of power (see stages from 0 to 25). On the contrary, it is used to provide the power of the load when the PV and the wind turbine cannot supply the required power, as can be observed in stages from 26 to 94. Finally, either the primary grid or the diesel generator can act as the last resource to compensate for the load, depending on their prices. Then, in stages 20 to 42 of Figure 9, the main grid's power was mostly used since it is the cheapest, as can be seen in Figure 10. On the contrary, in stages 43 to 70, the diesel generator's power was used because it has the lowest price.

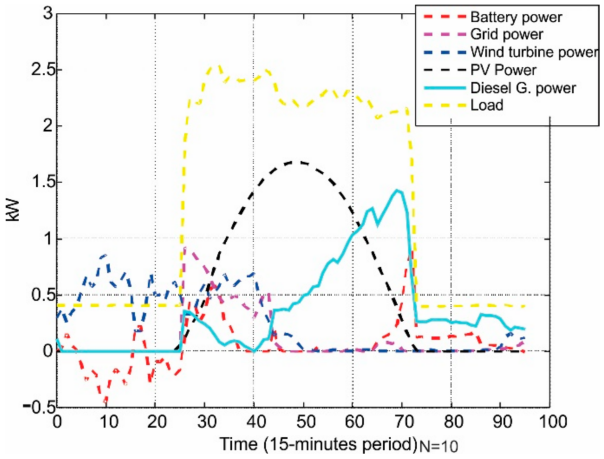

Figure 9. Forecasting power for the microgrid with N = 10.

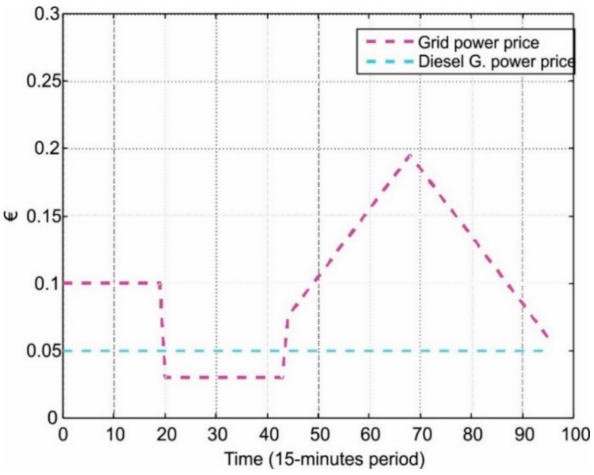

Figure 10. Generated power price [42].

Figure 11 summarizes the results of the state of charge of the storage system in the microgrid. As can be observed, in stages 1 and 2, the storage system was in discharge mode to compensate for the power t the wind turbine could not supply. From stage 3 to 15, the storage system charges up to 75%. Then, it delivers energy to the microgrid since the wind turbine reduces its production (see stages 16 and 17). From stage 18 to 26, it was charging until reaching 95%. Henceforth, the storage system only delivers power to the microgrid until 40% is discharged.

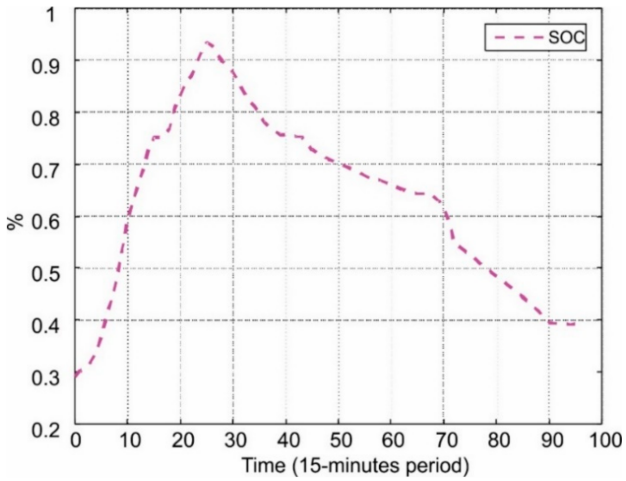

Figure 11. State of Charge (SOC).

For the sake of comparison, Figure 12 shows the microgrid's power cost for (i) the MPC method proposed in this work and (ii) the OPF (Optimal Power Flow) method, as previously proposed in the literature. The interested reader is referred to [41] for more details. The dashed magenta and blue lines represent the power management performed with the MPC and OPF techniques, respectively. As can be seen, the MPC method outperforms the results provided by OPF for the whole simulation, i.e., it obtains a better optimization of the power flows used in the microgrid, which stands to reduce the cost of power for the analyzed time stages.

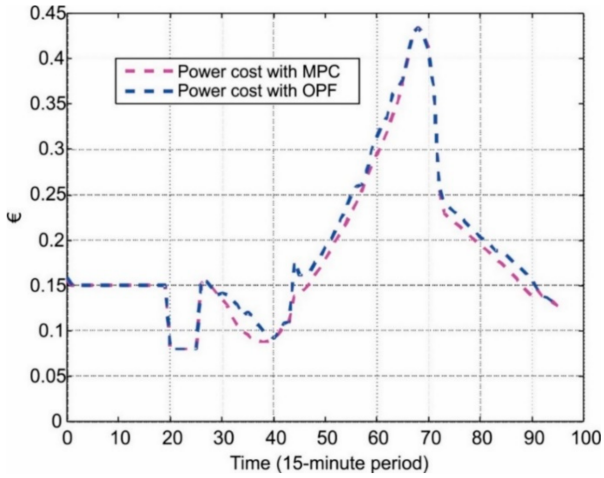

Figure 12. Power cost with MPC and OPF.

5. Conclusions

This work presents a controlled EMS under the MPC, incorporating solar radiation and wind speed predictions by using time series. Specifically, it uses the Double Exponential Smoothing (DES) method to predict both solar radiation and wind speed, and historical data. Since the DES prediction is combined with the MPC, the cost spent on energy from the main grid and the diesel generator is reduced, as the combination of the predictions and the control achieves a better performance in energy management. The obtained results have shown that the combination of an MPC with the DES predictions improves the performance of the conventional OPF techniques, reducing the error that introduces the uncertainty of solar photovoltaic systems and wind turbines. The benefit varies depending on the electric power tariff, the size of the ESS, and the size of the solar PV and wind systems. This work's main contribution is the integration of time series methods for the prediction of solar radiation and wind speed with MPC. In the future, EMS with MPC will be implemented in an experimental microgrid in the CIESOL Building to obtain real-time results of the EMS operation.

Author Contributions: Conceptualization, L.O.P.V. and J.D.Á.; formal analysis, L.O.P.V. and J.L.T.-M.; funding acquisition, V.M.R. and D.L.C.; investigation, L.O.P.V. and V.M.R.; methodology, D.L.C. and J.D.Á.; software, J.L.R.; supervision, V.M.R., J.L.R., J.L.T.-M. and J.D.Á.; writing—original draft, L.O.P.V.; writing—review & editing, J.D.Á. and J.L.R.; validation, L.O.P.V. All authors have read and agreed to the published version of the manuscript.

Funding: This research was funded by Consejo Nacional de Ciencia y Tecnología, grant number 2015-01-786 (Problemas nacionales), the International Joint Programming initiative of the State Research Agency of the Spanish Government, grant number PCI2019-103378 (Microgrids for solar self-supply in isolated productive environments, MICROPROD-SOLAR), the Spanish Ministry of Economy and Competitiveness (RTI2018-095993-B-I00), the Junta de Andalucía (FEDER-JA P18-FR-2378, P18-RT-1193), the University of Almería (UAL18-TIC-A020-B) and by the Iberoamerican Program for Science and Technology for the Development (CYTED).

Institutional Review Board Statement: Not applicable.

Informed Consent Statement: Not applicable.

Data Availability Statement: Not applicable.

Acknowledgments: The research of the authors was supported by Consejo Nacional de Ciencia y Tecnología, grant number 2015-01-786 (Problemas nacionales), the International Joint Programming initiative of the State Research Agency of the Spanish Government, grant number PCI2019-103378 (Microgrids for solar self-supply in isolated productive environments, MICROPROD-SOLAR), the Spanish Ministry of Economy and Com-petitiveness (RTI2018-095993-B-I00), the Junta de Andalucía

(FEDER-JA P18-FR-2378, P18-RT-1193), the University of Almería (UAL18-TIC-A020-B) and by the Iberoamerican Program for Science and Technology for the Development (CYTED).

Conflicts of Interest: The authors declare no conflict of interest.

Nomenclature

CF_T	Objective function
$h^{t_k}(x^{t_k})n^{t_i}$	Equality constrains.
$I_{CDm}^{t_k}$	Current at PV system terminals
$P_{Bcj}^{t_k}$	Battery charge power
$P_{Bdj}^{t_k}$	Battery discharge power
$P_{CDj}^{t_k}$	Photovoltaic system power
$p_{CDk}^{t_i}$	Panel terminal power
$P_{CDm}^{t_k}$	Power at PV system terminals
$P_{inj\ j}^{t_k}$	Active power injected of the microgrid
$P_{lj}^{t_k}$	Active Power of the load
$p_{lm}^{t_i}$	Load power
$P_{MGi}^{t_k}$	Main grid power
$P_{wj}^{t_k}$	Wind turbine power
$Q_{inj\ j}^{t_k}$	Reactive power injected of the microgrid
$Q_{MGj}^{t_k}$	Reactive power main grid
$Q_{lj}^{t_k}$	Reactive power of the load
$soc_{Sj}^{t_0}$	Initial state of charge
$SOC_{sj}^{tkt_i}$	State of charge
T	Time stages set
t_{ki}	Time stage
$V_{CDm}^{t_k}$	Voltage at PV system terminals
$yx^{t_{ki}}$	Variable Inequalities constraints
$z^{t_k}(x^{t_k})z^{t_i}$	Inequalities constraints

Appendix A

This appendix shows the parameters of the microgrid components which are:

Table A1. The parameters of the microgrid components.

	Battery	Loads	PV	Wind Turbine	G. Disel
Unit	1	1	1	1	1
kW	1	3	2	1	2
Volts	230 ± 5%	230 ± 5%	230 ± 5%	230 ± 5%	230 ± 5%

References

1. Lee, J.; Zhang, P.; Gan, L.K.; Howey, D.A.; Osborne, M.A.; Tosi, A.; Duncan, S. Optimal Operation of an Energy Management System Using Model Predictive Control and Gaussian Process Time-Series Modeling. *IEEE J. Emerg. Sel. Top. Power Electron.* **2018**, *6*, 1783–1795. [CrossRef]
2. Dkhili, N.; Eynard, J.; Thil, S.; Grieu, S. A survey of modelling and smart management tools for power grids with prolific distributed generation. *Sustain. Energy Grids Netw.* **2020**, *21*, 100284. [CrossRef]
3. Fichera, A.; Marrasso, E.; Sasso, M.; Volpe, R. Energy, Environmental and Economic Performance of an Urban Community Hybrid Distributed Energy System. *Energies* **2020**, *13*, 2545. [CrossRef]
4. Bordons, C.; García-Torres, F.; Valverde, L. Gestión Óptima de la Energía en Microrredes con Generación Renovable. *Rev. Iberoam. Automática Informática Ind. RIAI* **2015**, *12*, 117–132. [CrossRef]
5. Leonori, S.; Martino, A.; Frattale Mascioli, F.M.; Rizzi, A. Microgrid Energy Management Systems Design by Computational Intelligence Techniques. *Appl. Energy* **2020**, *277*, 115524. [CrossRef]

6. Banković, B.; Filipović, F.; Mitrović, N.; Petronijević, M.; Kostić, V. A Building Block Method for Modeling and Small-Signal Stability Analysis of the Autonomous Microgrid Operation. *Energies* **2020**, *13*, 1492. [CrossRef]
7. Olivares, D.E.; Mehrizi-Sani, A.; Etemadi, A.H.; Canizares, C.A.; Iravani, R.; Kazerani, M.; Hajimiragha, A.H.; Gomis-Bellmunt, O.; Saeedifard, M.; Palma-Behnke, R.; et al. Trends in Microgrid Control. *IEEE Trans. Smart Grid* **2014**, *5*, 1905–1919. [CrossRef]
8. Hooshmand, A.; Poursaeidi, M.H.; Mohammadpour, J.; Malki, H.A.; Grigoriads, K. Stochastic model predictive control method for microgrid management. In Proceedings of the 2012 IEEE PES Innovative Smart Grid Technologies (ISGT), Washington, DC, USA, 16–20 January 2012; pp. 1–7.
9. Cecilia, A.; Carroquino, J.; Roda, V.; Costa-Castelló, R.; Barreras, F. Optimal Energy Management in a Standalone Microgrid, with Photovoltaic Generation, Short-Term Storage, and Hydrogen Production. *Energies* **2020**, *13*, 1454. [CrossRef]
10. K/bidi, F.; Damour, C.; Grondin, D.; Hilairet, M.; Benne, M. Power Management of a Hybrid Micro-Grid with Photovoltaic Production and Hydrogen Storage. *Energies* **2021**, *14*, 1628. [CrossRef]
11. Morstyn, T.; Hredzak, B.; Agelidis, V.G. Dynamic optimal power flow for DC microgrids with distributed battery energy storage systems. In Proceedings of the 2016 IEEE Energy Conversion Congress and Exposition (ECCE), Milwaukee, WI, USA, 18–22 September 2016; pp. 1–6.
12. Dini, A.; Pirouzi, S.; Norouzi, M.; Lehtonen, M. Hybrid stochastic/robust scheduling of the grid-connected microgrid based on the linear coordinated power management strategy. *Sustain. Energy Grids Netw.* **2020**, *24*, 100400. [CrossRef]
13. Grüne, L. Approximation Properties of Receding Horizon Optimal Control. *Jahresbericht Dtsch. Math.* **2016**, *118*, 3–37. [CrossRef]
14. Numata, M.; Sugiyama, M.; Mogi, G. Barrier Analysis for the Deployment of Renewable-Based Mini-Grids in Myanmar Using the Analytic Hierarchy Process (AHP). *Energies* **2020**, *13*, 1400. [CrossRef]
15. Incremona, G.P.; Cucuzzella, M.; Magni, L.; Ferrara, A. MPC with Sliding Mode Control for the Energy Management System of Microgrids. *IFAC-PapersOnLine* **2017**, *50*, 7397–7402. [CrossRef]
16. Pawlowski, A.; Guzmán, J.L.; Rodríguez, F.; Berenguel, M.; Sánchez, J. Application of time-series methods to disturbance estimation in predictive control problems. In Proceedings of the 2010 IEEE International Symposium on Industrial Electronics, Bari, Italy, 4–7 July 2010; pp. 409–414.
17. Reikard, G. Predicting solar radiation at high resolutions: A comparison of time series forecasts. *Sol. Energy* **2009**, *83*, 342–349. [CrossRef]
18. Dev, S.; AlSkaif, T.; Hossari, M.; Godina, R.; Louwen, A.; van Sark, W. Solar Irradiance Forecasting Using Triple Exponential Smoothing. In Proceedings of the 2018 International Conference on Smart Energy Systems and Technologies (SEST), Seville, Spain, 10–12 September 2018; pp. 1–6.
19. Dong, Z.; Yang, D.; Reindl, T.; Walsh, W.M. Short-term solar irradiance forecasting using exponential smoothing state space model. *Energy* **2013**, *55*, 1104–1113. [CrossRef]
20. Soubdhan, T.; Ndong, J.; Ould-Baba, H.; Do, M.-T. A robust forecasting framework based on the Kalman filtering approach with a twofold parameter tuning procedure: Application to solar and photovoltaic prediction. *Sol. Energy* **2016**, *131*, 246–259. [CrossRef]
21. Zheng, Z.; Chen, H.; Luo, X. A Kalman filter-based bottom-up approach for household short-term load forecast. *Appl. Energy* **2019**, *250*, 882–894. [CrossRef]
22. Luan, H. Tran Application of Kalman Filtering for PV Power Prediction in Short-Term Economic Dispatch. Master's Thesis, College of Engineering and Mineral Resources, West Virginia University, Morgantownm, WV, USA, 2017.
23. Mayer, M.J.; Gróf, G. Extensive comparison of physical models for photovoltaic power forecasting. *Appl. Energy* **2021**, *283*, 116239. [CrossRef]
24. Ryan, A.G.; Regnier, C.; Divakaran, P.; Spindler, T.; Mehra, A.; Smith, G.C.; Davidson, F.; Hernandez, F.; Maksymczuk, J.; Liu, Y. GODAE OceanView Class 4 forecast verification framework: Global ocean inter-comparison. *J. Oper. Oceanogr.* **2015**, *8*, s98–s111. [CrossRef]
25. Premalatha, N.; Valan Arasu, A. Prediction of solar radiation for solar systems by using ANN models with different back propagation algorithms. *J. Appl. Res. Technol.* **2016**, *14*, 206–214. [CrossRef]
26. Arias-Rosales, A.; LeDuc, P.R. Modeling the transmittance of anisotropic diffuse radiation towards estimating energy losses in solar panel coverings. *Appl. Energy* **2020**, *268*, 114872. [CrossRef]
27. Vermuyten, E.; Meert, P.; Wolfs, V.; Willems, P. Combining Model Predictive Control with a Reduced Genetic Algorithm for Real-Time Flood Control. *J. Water Resour. Plan. Manag.* **2018**, *144*. [CrossRef]
28. Reynolds, J.; Rezgui, Y.; Kwan, A.; Piriou, S. A zone-level, building energy optimisation combining an artificial neural network, a genetic algorithm, and model predictive control. *Energy* **2018**, *151*, 729–739. [CrossRef]
29. Sarimveis, H.; Bafas, G. Fuzzy model predictive control of non-linear processes using genetic algorithms. *Fuzzy Sets Syst.* **2003**, *139*, 59–80. [CrossRef]
30. Clarke, W.C.; Manzie, C.; Brear, M.J. An economic MPC approach to microgrid control. In Proceedings of the 2016 Australian Control Conference (AuCC), Newcastle, NSW, Australia, 3–4 November 2016; pp. 276–281.
31. Batiyah, S.; Zohrabi, N.; Abdelwahed, S.; Sharma, R. An MPC-Based Power Management of a PV/Battery System in an Islanded DC Microgrid. In Proceedings of the 2018 IEEE Transportation Electrification Conference and Expo (ITEC), Long Beach, CA, USA, 13–15 June 2018; pp. 231–236.
32. Romero-Quete, D.; Garcia, J.R. An affine arithmetic-model predictive control approach for optimal economic dispatch of combined heat and power microgrids. *Appl. Energy* **2019**, *242*, 1436–1447. [CrossRef]

33. Camacho, E.F.; Bordons, C. *Model Predictive Control*, 2nd ed.; Advanced Textbooks in Control and Signal Processing; Michael, J., Grimble, M.A.J., Eds.; Springer: London, UK, 2007; ISBN 978-1-85233-694-3.
34. Mayne, D.Q.; Rawlings, J.B.; Rao, C.V.; Scokaert, P.O.M. Constrained model predictive control: Stability and optimality. *Automatica* **2000**, *36*, 789–814. [CrossRef]
35. Delfino, F.; Ferro, G.; Minciardi, R.; Robba, M.; Rossi, M.; Rossi, M. Identification and optimal control of an electrical storage system for microgrids with renewables. *Sustain. Energy Grids Netw.* **2019**, *17*, 100183. [CrossRef]
36. Petrollese, M.; Valverde, L.; Cocco, D.; Cau, G.; Guerra, J. Real-time integration of optimal generation scheduling with MPC for the energy management of a renewable hydrogen-based microgrid. *Appl. Energy* **2016**, *166*, 96–106. [CrossRef]
37. e Silva, D.P.; Félix Salles, J.L.; Fardin, J.F.; Rocha Pereira, M.M. Management of an island and grid-connected microgrid using hybrid economic model predictive control with weather data. *Appl. Energy* **2020**, *278*, 115581. [CrossRef]
38. Yassuda Yamashita, D.; Vechiu, I.; Gaubert, J.-P. Two-level hierarchical model predictive control with an optimised cost function for energy management in building microgrids. *Appl. Energy* **2021**, *285*, 116420. [CrossRef]
39. Ahmadi, S.E.; Rezaei, N.; Khayyam, H. Energy management system of networked microgrids through optimal reliability-oriented day-ahead self-healing scheduling. *Sustain. Energy Grids Netw.* **2020**, *23*, 100387. [CrossRef]
40. Nelson, J.R.; Johnson, N.G. Model predictive control of microgrids for real-time ancillary service market participation. *Appl. Energy* **2020**, *269*, 114963. [CrossRef]
41. Polanco Vasquez, L.O.; Carreño Meneses, C.A.; Pizano Martínez, A.; López Redondo, J.; Pérez García, M.; Álvarez Hervás, J.D. Optimal Energy Management within a Microgrid: A Comparative Study. *Energies* **2018**, *11*, 2167. [CrossRef]
42. OMIE. Available online: https://www.omie.es/es/sobre-nosotros (accessed on 22 December 2020).
43. Pérez-García, M.; Castilla, M.M.; Álvarez, J.D.; Ruano, A.E.; Pérez-García, M. Characterization of an Energy Consumption Model for a Net Zero Energy Building Laboratory. In Proceedings of the EuroSun2016, Palma de Mallorca, Spain, 11–14 October 2016; International Solar Energy Society: Freiburg, Germany, 2016; pp. 1–11.